Downloaded from orbit.dtu.dk on: May 05, 2023

DTU Library

Effective roughness and displacement height over forested areas, via reduced-dimension CFD

Sogachev, Andrey; Cavar, Dalibor; Kelly, Mark C.; Bechmann, Andreas

Publication date:
2017

Document Version
Publisher's PDF, also known as Version of record

Link back to DTU Orbit

Citation (APA):
Sogachev, A., Cavar, D., Kelly, M. C., & Bechmann, A. (2017). *Effective roughness and displacement height over forested areas, via reduced-dimension CFD*. DTU Wind Energy E Vol. 0161

General rights
Copyright and moral rights for the publications made accessible in the public portal are retained by the authors and/or other copyright owners and it is a condition of accessing publications that users recognise and abide by the legal requirements associated with these rights.

- Users may download and print one copy of any publication from the public portal for the purpose of private study or research.
- You may not further distribute the material or use it for any profit-making activity or commercial gain
- You may freely distribute the URL identifying the publication in the public portal

If you believe that this document breaches copyright please contact us providing details, and we will remove access to the work immediately and investigate your claim.

Effective roughness and displacement height over forested areas, via reduced-dimension CFD

Department of Wind Energy E Report 2017

Andrey Sogachev, Dalibor Cavar, Mark Kelly, Andreas Bechmann

DTU Wind Energy E-0161

December 2017

DTU Wind Energy
Department of Wind Energy

Authors: Andrey Sogachev, Dalibor Cavar, Mark Kelly, Andreas Bechmann
Title: Effective roughness and displacement height over forested areas, via reduced-dimension CFD
Department: DTU Wind Energy

Summary (max 2000 characters):
While extensive field campaigns as well as modern remote sensing methods based on airborne laser scans allow obtaining of detailed information about forest canopy structure, there is still a great need for simple and consistent description of vegetation roughness, as its parametrization differs significantly from one flow model to the other (e.g. CFD, mesoscale and linearized models). Here, we present a method to facilitate use of forest data, having an arbitrary level of detail, in flow models employing different types or levels of canopy drag-force prescription.

DTU Wind Energy E-0161
December 2017

ISBN 978-87-93549-29-6

Pages: 35
Figures: 22
References: 36

Technical University of Denmark
Department of Wind Energy
Frederiksborgvej 399
Building 118
4000 Roskilde
Denmark
Telephone +4521331197
anso@dtu.dk

www.vindenergi.dtu.dk

Content

Summary

While extensive field campaigns as well as modern remote sensing methods based on airborne laser scans allow obtaining of detailed information about forest canopy structure, there is still a great need for simple and consistent description of vegetation roughness, as its parametrization differs significantly from one flow model to the other (e.g. CFD, mesoscale and linearized models). Here, we present a method to facilitate use of forest data, having an arbitrary level of detail, in flow models employing different types or levels of canopy drag-force prescription.

1. Introduction

The lack of accurate information about forest canopy structure currently limits the accuracy of numerical predictions of the wind field over forested terrain. While forest has commonly been represented via roughness length and displacement height in wind models, these parameters have often been defined in subjective ways without relation to the actual forest structure at a given site (e.g. Raupach, 1994). Alternatively, the canopy structure in Computational Fluid Dynamics (CFD) can be specified directly through the Plant Area Density (PAD) for each grid volume in a three-dimensional (3D) model domain. Advanced CFD models capable of incorporating (distributed) local drag forces have attained widespread use in wind energy, so proper application of PAD measurements becomes highly important. Here we consider methods to parameterize the PAD description including translation into roughness aiming to facilitate use of such forest data in flow models with different types or levels of canopy drag-force prescription (e.g. CFD, mesoscale and linearized models); it also allows comparison with known theory, measurements, and commonly used parameters in forest-flow modelling.

2. Derivation and parameterization of PAD

2.1 Statistical approach

The information about PAD can be derived by different methods. In traditional forestry, most structural properties — like tree height, crown width, crown length, etc. — have been related by allometric relationships to an easily measurable primary variable. In most cases this variable is the Diameter-at-Breast-Height (DBH) i.e., the diameter of the tree trunk at a height of 1.37 m above the ground. Based on this parameter *h* (tree height) and PAI (plant area index) for different spices can be estimated (see Widlowski et al., 2003; Picard et al., 2012). Plant Area Density is related to the Plant Area Index (PAI) by

$$\mathrm{PAI} = \int_0^h \mathrm{PAD}(z)dz \ , \tag{1}$$

where *z* is the height above the ground.

Field experiments also provide detail information about tree properties including vertical foliage distribution (e.g. Ross, 1981; Breuer et al., 2003). Another possibility to derive vegetation height is to use digital elevation map. Considering the difference between topography and elevation data one can estimate the height of object over ground level, including the vegetation height. Based on this information some robust assumptions about the PAD can be done (Mann et al., 2010; Sogachev et al., 2015). Nowadays airborne laser scans are becoming a more popular method of getting the information about vegetation properties. Methods allowing to calculate highly heterogeneous and realistic PAD from LiDAR scan data are developed (Lefsky et al., 1999; Solberg et al., 2006; Morsdorf et al, 2006; Richardson et al., 2009; Boudreault et al., 2015). While such PAD data is in principle applicable to CFD models handling high-resolution

input, such data must presently be processed in order to be usable for general wind flow modelling.

To use detailed information about forest in the model, one usually apply a statistical approach in an attempt to order frontal density data into a number of land-use classes, before describing the mean properties within each. Accordingly, based on forest height information the vegetation is subdivided in classes. After that each height class is used to derive the PAI value. Statistical analysis of LiDAR scan data can easily provide mean values for each height class as well as the mean shape of foliage. If LiDAR scan data is unavailable, the PAI and PAD can be estimated using above mentioned allometric relationships of traditional forestry.

2.2 Empirical method

Independent of the method for derivation of PAD and in order to facilitate its usage in the models, one usually utilize the two well-known empirical methods of description of normalized PAD profiles through a number of simple parameters: one based on the beta-distribution (Meyers and Paw U ,1986), and one suggested by Lalic and Michailovic (2004). Both methods consider mean values of h and z_m (the height where maximum plant area density PAD_m occurs) in each class as key parameters in the definition of the vertical plant structure. The beta probability density function, formulated as follows:

$$\mathrm{PAD}(z) = \mathrm{PAI}\left[\left(\frac{z}{h}\right)^{\alpha-1}\left(1-\frac{z}{h}\right)^{\beta-1}\right]\left[\int_0^h \left(\frac{z}{h}\right)^{\alpha-1}\left(1-\frac{z}{h}\right)^{\beta-1} dz\right]^{-1}, \quad (2)$$

has been used previously to represent profiles of plant area density (e.g. Meyers and Paw U, 1986; Markkanen et al., 2003) or source distribution (e.g. Van Den Hurk and McNaughton, 1995) inside the canopy. The mode of a beta-distributed random variable with parameters α, β > 1 is the most likely value of the distribution (corresponding to the peak in the PDF) and is given by:

$$M = \frac{\alpha - 1}{\alpha + \beta - 2}. \quad (3)$$

Thus, using (2) with $M = z_m/h$, one can easily examine the effect of different canopy densities and structures on the scalar and flow dynamics. Two parameters (α, β) determine the shape of the distribution. For example, when $\alpha > \beta$ the maximum value occurs at $z/h > 0.5$, corresponding to a region of maximum foliage (or a source) concentrated in the upper part of the canopy. For given z_m/h and β value we can estimate α from:

$$\alpha = \left(\frac{z_m}{h}(\beta - 2) + 1\right)\left(1 - \frac{z_m}{h}\right)^{-1}. \quad (4)$$

Thus to find α and β for a given height class, we have to iteratively solve the set of equations (2) and (4) until the best correspondence between $PAD(z_m)$ and PAD_m is obtained.

Applying a mathematical procedure established by Plank (see Lalic and Michailovic (2004) and references therein), Lalic and Michailovic (2004) also found that PAD(z) can approximately be described by a function of the following form:

$$\mathrm{PAD}(z) = \mathrm{PAD}_{\mathrm{m}}\left(\frac{h - z_m}{h - z}\right)^{\gamma} \exp\left[\gamma\left(1 - \frac{h - z_m}{h - z}\right)\right], \qquad (5)$$

where

$$\gamma = \begin{cases} 6.0 & 0 \le z \le z_m \\ 0.5 & z_m \le z \le h. \end{cases}$$

This function was validated against plant area density observations from eight sites located in four different types of forest, covering a broad range of mean values of PAI between 2 and 18.

Figure 1 shows that two empirical methods result in different vertical plant area profiles even for vegetation with the same PAI and same location of maximum foliage. The difference becomes small for z_m/h higher than 0.8.

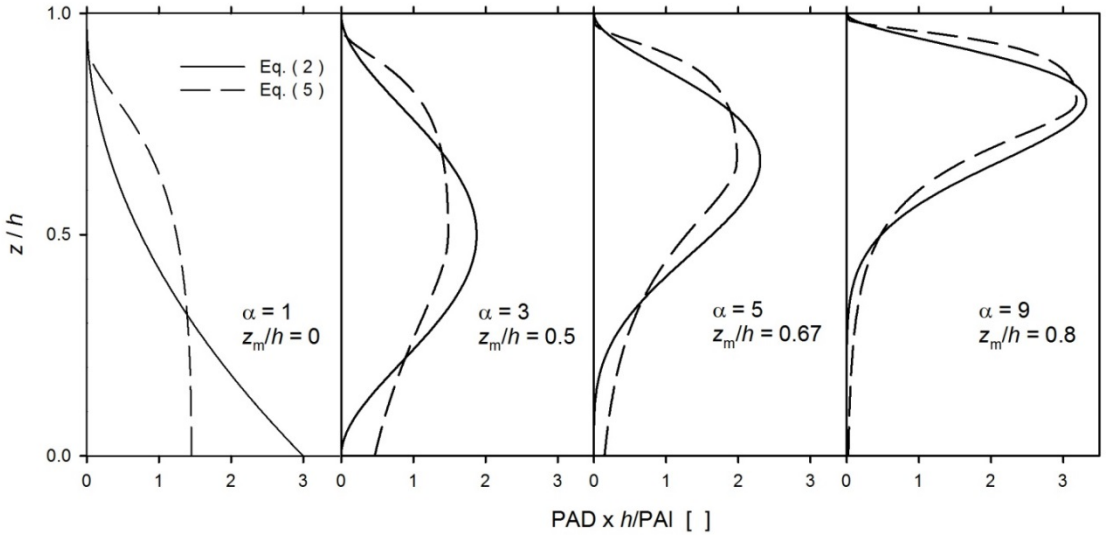

Figure 1. *Normalized vertical profiles of foliage density for different forest architectures described according to Eq. (2) (solid lines) with varied α and fixed β at β = 3 and according to Eq. (5) (dashed lines) with z_m/h derived from Eq.(4) for α and β used in Eq. (2).*

3. Translating PAD to effective roughness and displacement height

3.1 Estimation of effective roughness

Here we present a novel approach using the SCADIS solver — an Atmospheric Boundary Layer (ABL) code capable of simulating canopy flows (Sogachev et al., 2002; Sogachev, 2009), in order to estimate the effective aerodynamic roughness length, $z_{0,eff}$ — thereby describing each land-use class with a single parameter. SCADIS provides steady-state profiles of velocity components, turbulent kinetic energy, dissipation rate and the mean momentum flux for specified geostrophic wind, G, latitude and a predefined canopy drag. Thus, the "geostrophic drag law" (e.g., Blackadar and Tennekes, 1968) is implicitly applied, which, combined with Rossby number similarity theory, gives the following geostrophic wind in the neutral, barotropic boundary layer:

$$G = \frac{u_*}{\kappa}\left[\left(\ln\frac{u_*}{f\,z_{0,eff}} - A\right)^2 + B^2\right]^{1/2}. \qquad (6)$$

Thus

$$z_{0,eff} = \frac{u_*}{f}\exp\left\{-\left[\left(\left(\frac{\kappa G}{u_*}\right)^2 - B^2\right)^{1/2} + A\right]\right\}. \qquad (7)$$

In equations (6) and (7) κ is the von Kármán constant (usually accepted to be 0.4), f is the Coriolis parameter, u_* is the friction velocity at the 'virtual' surface (generally the mean tree top height). The geostrophic component coefficients {A, B} have historically been established empirically via ABL measurements (Melgarejo and Deardorff, 1974; Clarke and Hess, 1974). Our calculations used A = 1.8 as in Troen and Peterson (1989) and wind energy practice (roughly equal to the mean of values found in literature). The value B = 6.4 is fitted to match solutions of SCADIS with drag forces and $z_{0,eff}$, and is slightly higher than the mean value of B given by Troen and Peterson (1989) (see Section 7 for discussion). In calculations, G is taken as 10 m s^{-1} and f is specified in accordance to the location of the test site (see below).

3.2 Derivation of displacement height and aerodynamic roughness

Use of the $z_{0,eff}$ parameter allows us to predict airflow over a surface covered by the vegetation using a flow model, without explicitly resolving the canopy drag. In order to describe the mean wind U above a surface covered by a vegetative canopy, using similarity theory, a displacement height (d) is needed in addition to the aerodynamic roughness length (z_0):

$$U(z) = \frac{u_*}{\kappa} \ln\left(\frac{z-d}{z_0}\right). \tag{8}$$

Note that z_0 is not the same as $z_{0,eff}$. Expression (8) implies that the flow should be "deflected" upwards in such a way that the mean flow properties above a vegetative canopy (forest), beginning roughly from a height *d* within the forest, are similar to those above the open flat ground. There are several approaches to estimating *d* and z_0 from only forest parameters, i.e. the tree height and PAI (Raupach, 1992; 1994). They are quite simple to use, but lack validation against real field conditions. These approaches do not account for the vertical vegetation structure either and suffer from a need to specify several fitting parameters. Therefore, we again apply SCADIS simulations to estimate *d* and z_0, following Sogachev and Kelly (2016):

$$d = h - \frac{u_{*h}}{\kappa (dU/dz)_h}, \tag{9}$$

$$z_0 = (h-d)\exp\left(\frac{\kappa U(h)}{u_{*h}}\right), \tag{10}$$

where subscript *h* refers to the canopy-top values. Although expression (8), as we will see below, allows only for estimation of *U* in the shallow layer above the canopy, we estimate *d* and z_0 as a unique set of parameters for each of the specified classes.

3.3 Data filtering

Specified only in the 2D horizontal space, the parameters $z_{0,eff}$, *d* and z_0 can be smoothed or aggregated for potential application. To do that, we use a bilateral filter, which is a non-linear edge-preserving and noise-reducing smoothing operator, originally introduced by Tomasi and Manduchi (1998) for images. The intensity value of each pixel in an image, *g(i, j)*, is replaced by a weighted average of intensity values from nearby pixels, *φ*(*l, m*),

$$g(i,j) = \frac{\sum_{l,m} \varphi(l,m)\omega(i,j,l,m)}{\sum_{l,m} \omega(i,j,l,m)}. \tag{11}$$

This weight can be based on a Gaussian distribution. Also, the weight depends not only on Euclidean distance of pixels (*a spatial or domain kernel*),

$$s(i,j,l,m) = \exp\left(-\frac{(i-l)^2 + (j-m)^2}{2\sigma_s^2}\right), \tag{12}$$

but also on the radiometric differences (e.g. range differences, such as color intensity, depth distance or as in our case $z_{0,eff}$, *d* and z_0 — *a data-dependent range kernel*)

$$r(i,\, j, l, m) = \exp\left(-\frac{\left\| \varphi(i,\, j) - \varphi(l, m) \right\|^2}{2\sigma_r^2} \right). \tag{13}$$

Multiplying expressions (12) and (13) one obtains the data-dependent bilateral weight-function:

$$\omega(i,\, j, l, m) = \exp\left(-\frac{(i-l)^2 + (j-m)^2}{2\sigma_s^2} - \frac{\left\| \phi(i,\, j) - \phi(l, m) \right\|^2}{2\sigma_r^2} \right). \tag{14}$$

As the range parameter σ_r increases, the bilateral filter gradually approaches the Gaussian convolution more closely, because the range Gaussian (*r*) widens and flattens, becoming nearly constant over the intensity interval of the 'image' (here aerodynamic properties of canopy/class area). As the spatial parameter σ_s increases, most of the "minor" features get smoothened out.

4. Numerical experiments

As mentioned above, ABL model SCADIS (Sogachev et al., 2002; Sogachev, 2009) in its one-dimensional mode is a basic tool for translating the PAD into the effective roughness and displacement height. SCADIS in its two or three-dimensional mode also allows airflow estimation over complex terrain. However, the model is designed for a single processor use and cannot be utilized on a massive computing scale, needed in the wind industry. Another DTU Wind Energy's in-house CFD solver — EllipSys3D (e.g. Michelsen, 1992; Sørensen, 2003) have however been designed for massive parallel computing. Both models apply the two-equation closure approach based on coupled transport equations for the turbulent kinetic energy (TKE), *k*, and a supplementary length-scale determining variable φ ($\varphi = \varepsilon$, ω, where ε is the dissipation rate of turbulent kinetic energy, *k*, and $\omega = \varepsilon/k$ is the specific dissipation) (e.g. Pope, 2000). In the present work both models will be used for test of the method: SCADIS only with k - ω turbulent closure and EllypSys3D with k - ω and k - ε closures.

The SCADIS solution is based on a finite difference numerical approach, while EllipSys3D utilizes a finite volume numerical method. To make results comparable, we used an upwind discretization scheme for the advection term in EllipSys3D, as this is the only option in SCADIS. An initial condition for wind speed was also identical and specified for flat plain terrain with aerodynamic roughness of 0.03 m, with western geostrophic wind of G = 10 m s^{-1}, at the upper border of the modelling domain (2 km in SCADIS and 5 km in EllipSys3D).

Calculations were conducted first with full description of canopy drag (for the method see Sogachev et al., 2012; 2015) and after that with effective roughness replacing the vegetation.

5. Case study

The Østerild National Test Centre for Large Wind Turbines is located on a coastal plain, in northern Jutland, Denmark (http://www.vindenergi.dtu.dk/english/test-centers/oesterild). Figure 2 shows digital topography map (DTM) (Fig. 2a) and digital surface map (DSM) (Fig.2b) from a national topography database (DHM – Danmarks Højdemodel, http://download.kortforsyningen.dk) before the test centre was build and part of forest surrounding it was cut. The terrain is flat, except for a small hill in the southwest direction and some sand dunes to the north. The elevations of the test area range from approximately 12 to 14 m ASL. The surroundings are dominated by the North Sea, which is approximately 4 km to the north and 20 km to the west. There is also the Limfjord entrance about 6 km to the southeast. The site has grasslands, and forests in the southern half of the test site with canopy heights between 10 m and 20 m. The original data set provides the horizontal resolution as 1.6 m. To demonstrate method and to speed-up data processing we use here the resolution of 16 m.

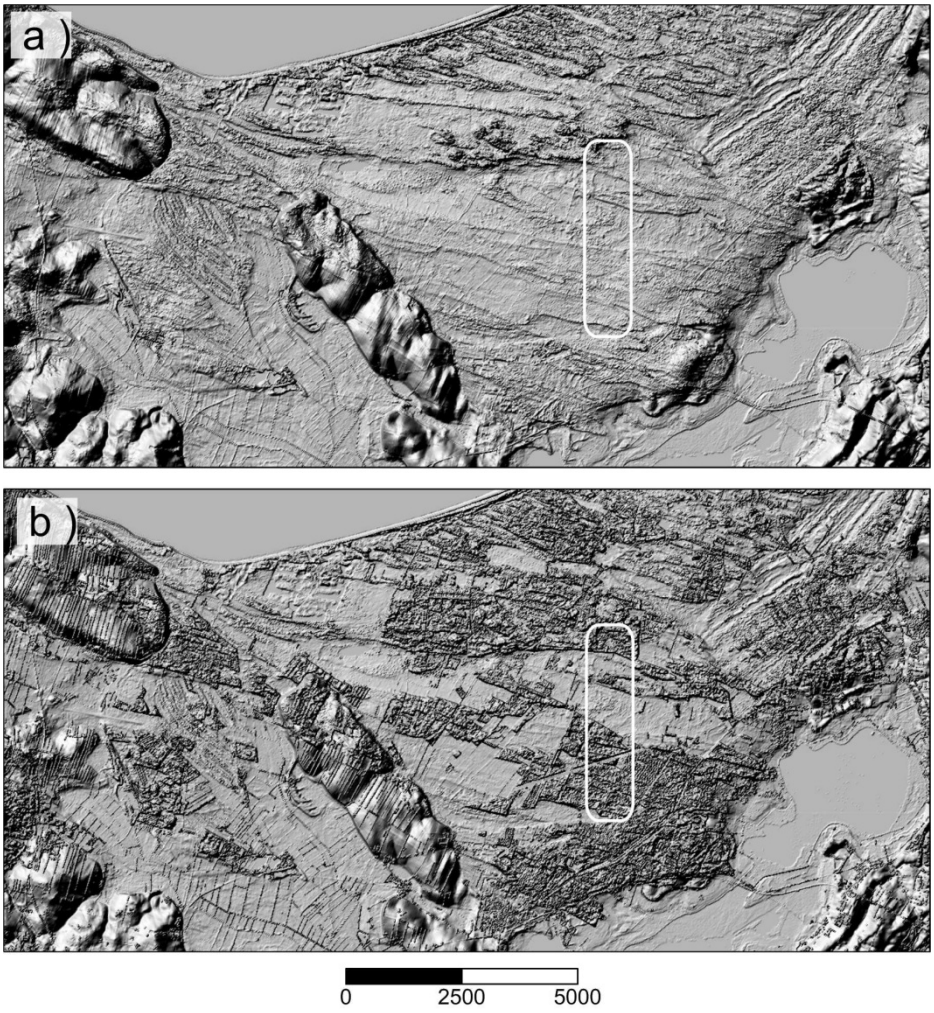

***Figure 2**. DTM (a) and DSM (b) of Østerild area. White line contours the area of the Østerild National Test Centre.*

6. Results

6.1 Forest height, PAI, PAD and effective roughness around Østerild test station

The base for derivation of effective roughness over Østerild site is the height of objects over the ground (Fig.3), which is derived as difference between DSM and DTM datasets. There are few artificial objects in this area, thus the assumption that difference between DSM and DTM is the horizontal distribution of the tree height was utilized. In earlier works the vegetation, for simplicity, was ranked in seven height classes with assumed constant PAI and with PAD given by Eq. (2) with a priori assumption of α and β parameters. Such land use classes were used in modelling for preliminary assessments of landscape on airflow over expected position of the Test Centre in Mann et al. (2010) and to test and validate the performance of EllipSys3D model after implementation of canopy parameterization (Sogachev at. al. 2015).

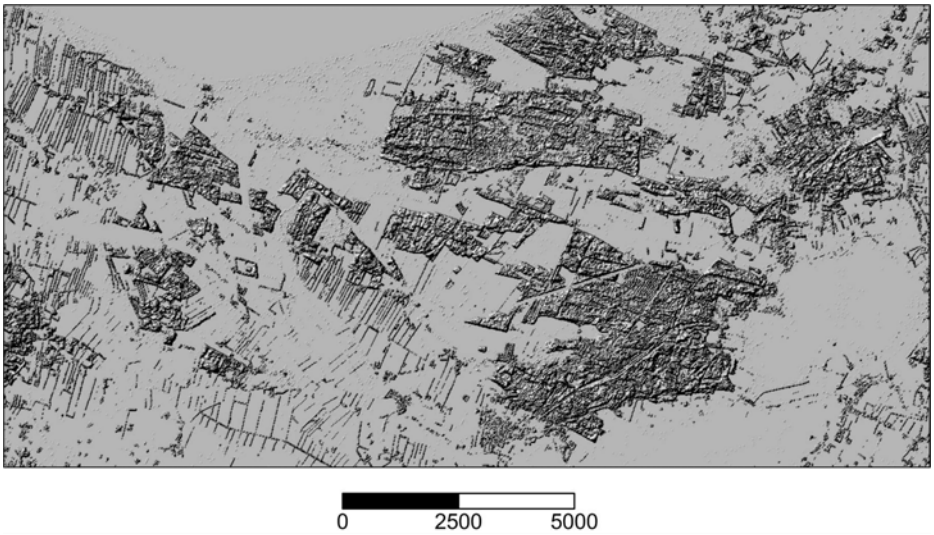

***Figure 3**. Map of objects over ground surface.*

In the present work plant heights were binned (rounding to the nearest integer value of h), and assigned to a class N (henceforth N = h). PAI and PAD for each class (or rounded height) were derived using allometric relationships for predominant tree type over Østerild test station (see Appendix A). Figure 4 show horizontal distribution of rounded heights of trees and PAI. Figure 5 shows the PAD profiles derived using allometric relationships that now can be used for derivation of aerodynamic parameters.

CFD simulations using the full description of canopy drag forces (Figs. 6 and 7: Canopy drag) and simulations using the effective roughness (Figs. 6 and 7: $z_{0,eff}$) indicate that the major difference is observed in the near-surface layer. The height of this layer depend on the vertical structure of vegetation and can be varied from 20 m (about $2h$ - when $z_{0,eff}/h > 0.1$) until 200 m

(about 10*h* - when $z_{0,eff}/h < 0.04$) (see also Fig. 9). Above this height, the ABL wind profiles derived by the different methods converge. Local friction velocities are also identical, except in the canopy layer. The logarithmic 'deflected' profile of wind speed is in a good accordance with the full canopy drag solution only in a very shallow layer near the canopy top. For the purposes of wind energy, it is quite clear that the solution based on the new CFD method of determining $z_{0,eff}$ is preferable. Figure 8 shows horizontal distribution of effective roughness over investigated area. The roughness was derived for trees with PAD presented in Fig. 5. Referring to data presented in Fig. 4b one can see that the area of higher LAI has lower roughness due to forest architecture based on allometric relationships.

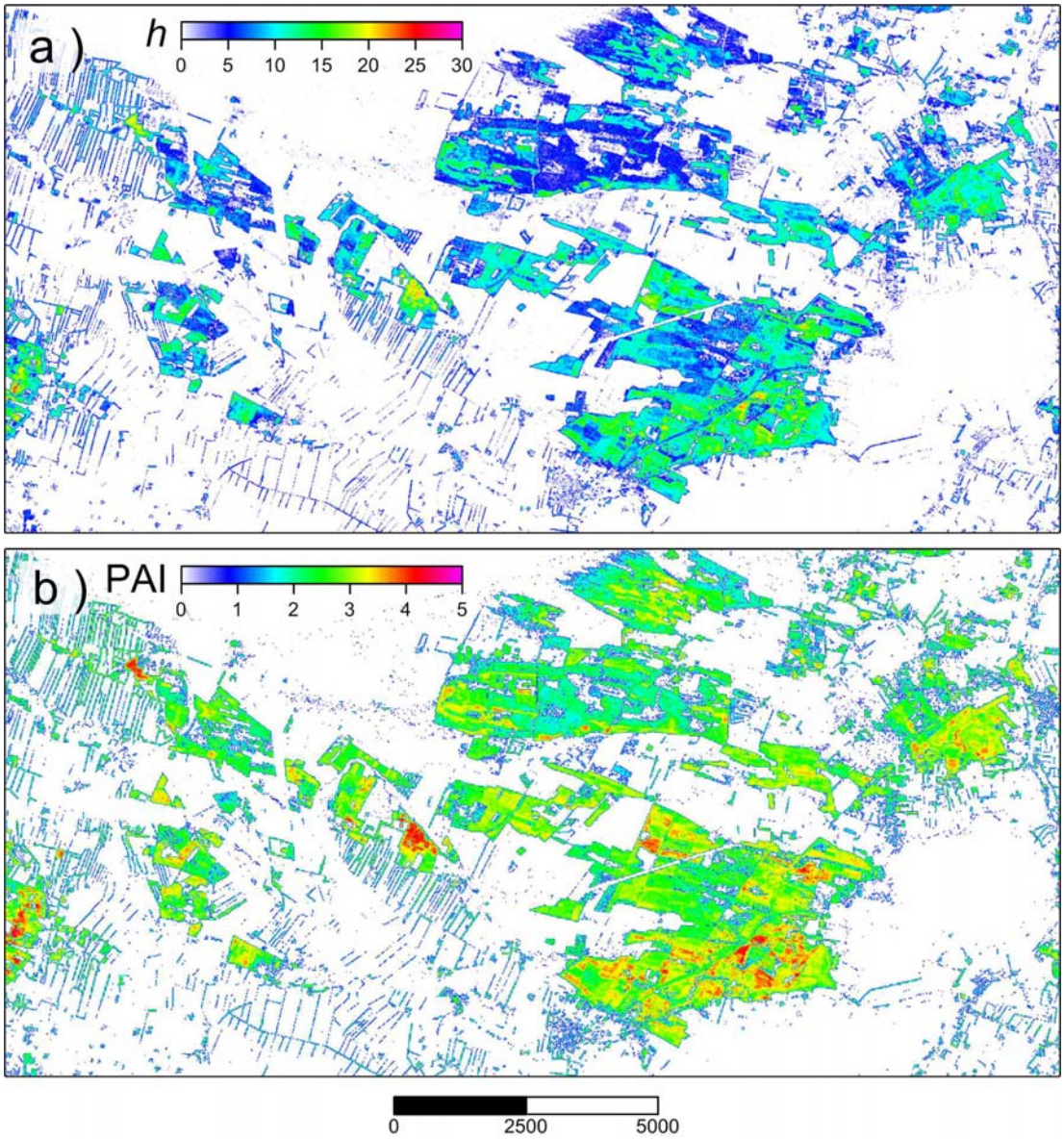

***Figure 4**. Horizontal distribution of rounded heights of tree h (m) (a) and PAI (m^2 m^{-2}) (b).*

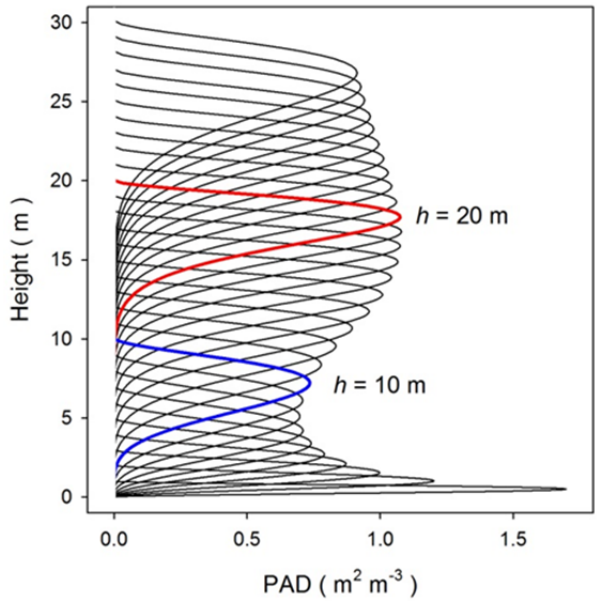

***Figure 5**. PAD profiles for trees of different height derived using allometric relationships for Scots Pine (see Appendix A). Blue and red lines indicate the profile for tree heights of 10 m and 20 m, respectively*

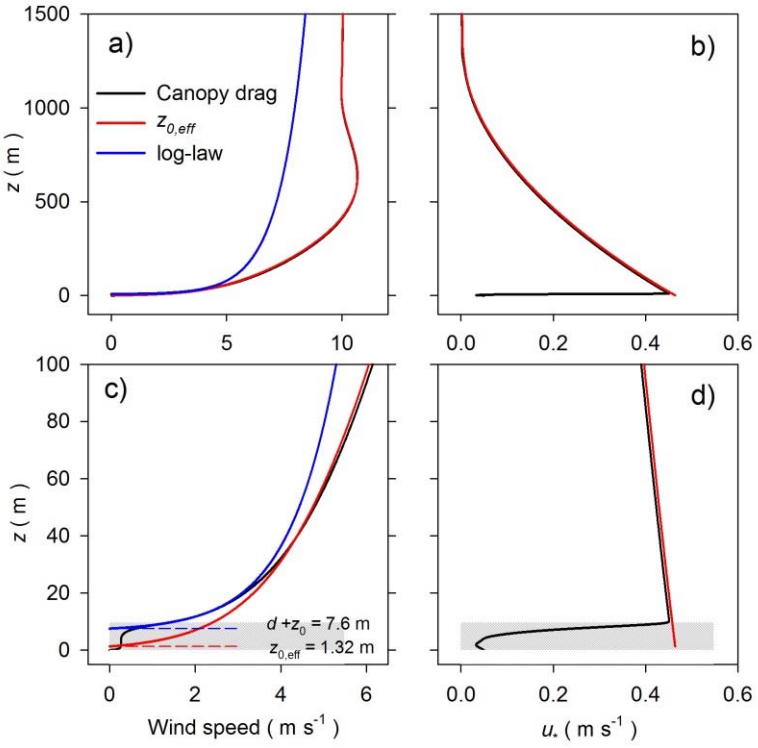

***Figure 6**. Wind speed (a and c) and the dynamic friction velocity (b and d) in ABL (upper panels) and in the surface layer (bottom panels) modelled by SCADIS using canopy drag (black lines) and effective roughness (red lines) for forest height h = 10 m (G = 10 m s^{-1}) (indicated in Fig. 5 by blue line). Logarithmic displaced wind profiles (blue lines) based on d and z_0 derived from SCADIS with the canopy drag is also shown (a and c). Shaded areas indicate canopy. The levels of d + z_0 and $z_{0,eff}$ where the wind speed takes zero value are shown in (c).*

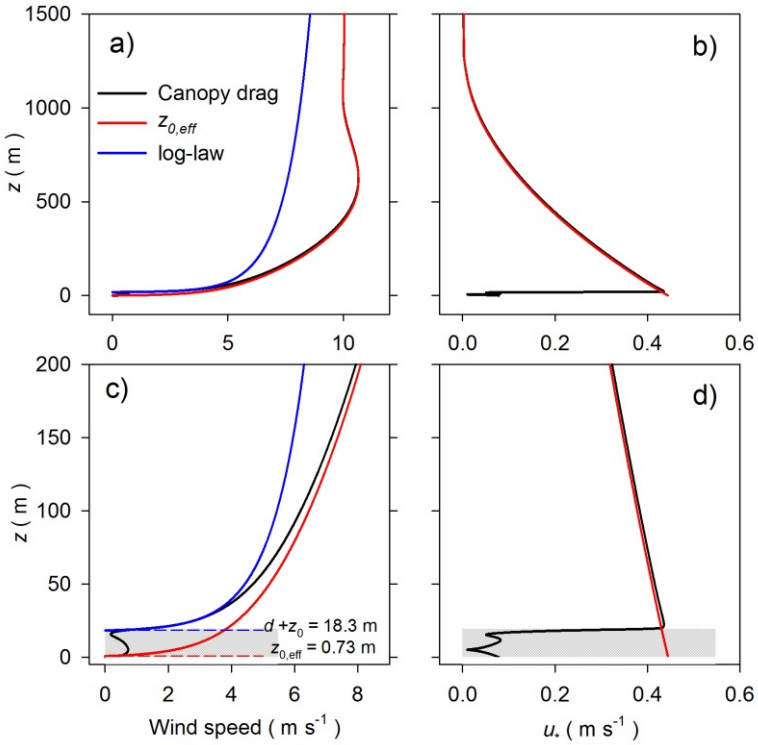

Figure 7. *The same as in Fig. 6 except for forest height h = 20 m (indicated in Fig. 5 by red line).*

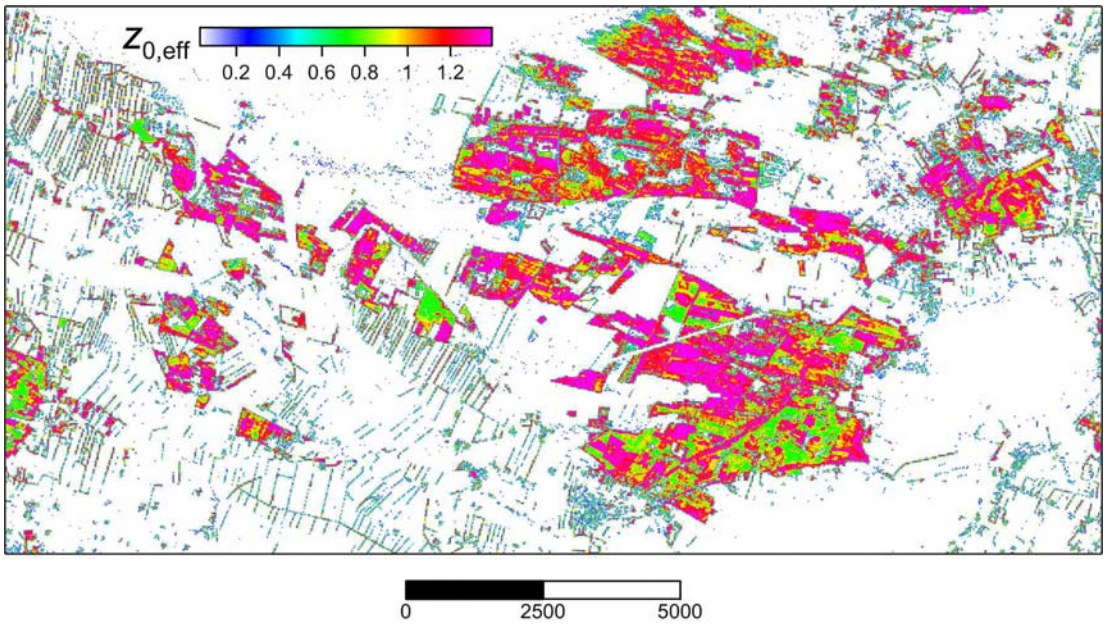

Figure 8*. Horizontal distribution of effective roughness* $z_{0,eff}$ *(m).*

Results of the sensitivity test with different shapes of PAD show that the effective roughness, i.e. dynamical resistance of the underlying surface, depends on the vertical foliage distribution for given *h* and PAI (Fig. 9). When foliage is mostly located in the lower or in the middle part of a tree ($\alpha < 5$) (for shape see Fig. 1) the roughness is growing with increase in the tree height, or with growing PAI. When foliage is located in the upper part ($\alpha > 5$) behaviour of the effective roughness depending on the tree height and PAI becomes more unpredictable. For our case with PADs presented in Fig. 5 the effective roughness grows with increase in the tree height until tree height of 8 m, after that gradually decreases and reaches approximately a constant value ($z_{0,eff} \approx 0.7$ m) for trees higher than 15 m. The sensitivity test shows that the knowledge about the real vertical foliage profile is very important for correct estimation of aerodynamic properties of vegetation.

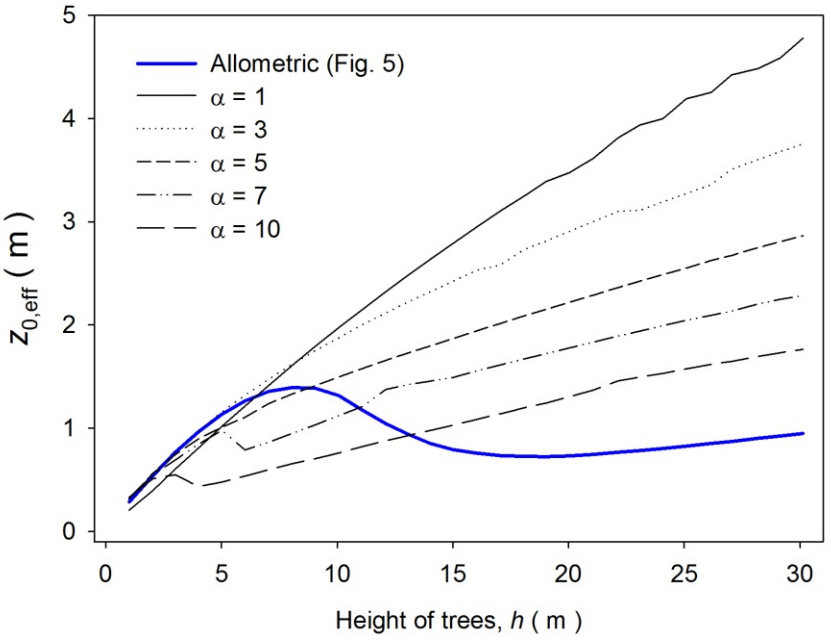

***Figure 9**. Effect of different assumption about PAD on effective roughness. Blue line for $z_{0,eff}$ derived using PAD profiles based on allometric relationships (see Fig. 5). Black lines for $z_{0,eff}$ derived using PAD profiles described by Eq. (2) with varied α and fixed β at β = 3 (see Fig. 1). In all cases the same class of tree height has the same PAI.*

The goal of the present work is not to estimate real surface properties over investigated area but to demonstrate the method of PAD translation into the effective roughness. PAD derived from allometric relationships provide an effective roughness range over the area until 1.5 m (Fig. 8). To provide a more clear effect of the effective roughness on the airflow modelling it will be desirable to have a wider range of this parameter. At the same time the vertical shape of a tree should still be close to the realistic one. The compromise here can be the choice of the tree shape with $z_m/h = 0.5$ and $\alpha = 3$ (see Fig. 1 for the PAD shape).

The horizontal distribution of the effective roughness over a limited domain with new derived PAD is given in Fig. 10a. The domain shown presents the most forested part of the initial area and has minor variation in topography. Using this domain size of about 7 km x 7 km in modelling allows us to consider only the effect of different forest representations on the airflow. For modelling purposes forest height gradually decreases to zero at borders of the domain. Those buffer zones are 500 m wide. This also implies that the effective roughness gradually attain the roughness value for plane ground (z_0 = 0.03 m) at the domain borders. Considering the limited domain allows us also to better visualise how the effective roughness varies in space. For some application the high variability of the parameter can be improper, and then we advise to apply the bilateral filter (Section 3.3) for smoothing the parameters over the considered area. An example of such filtering is given in Fig. 10b. One can see that small details are smoothed out, but the 'big picture' (primary features) are still captured (e.g. in comparison to figure 10a).

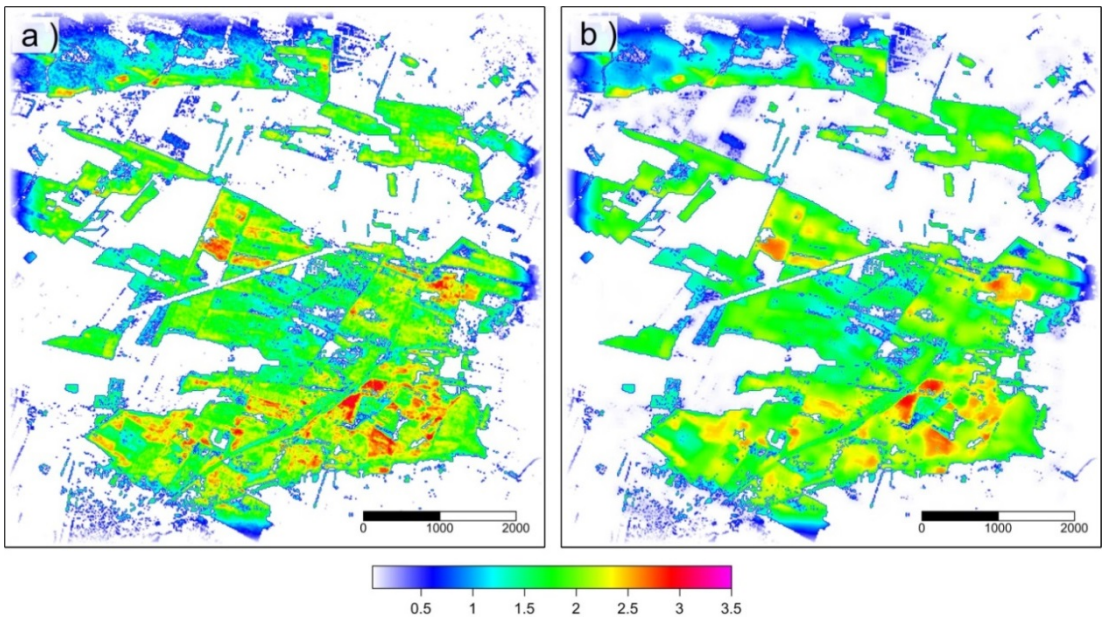

***Figure 10**. The effective aerodynamic roughness length, $z_{0,eff}$ (m) estimated for a limited area (a). The results of application of bilateral filter to original $z_{0,eff}$ with σ_s = 50 m and σ_r = 0.5 m is also shown in (b) (see text for details).*

6.2 Effect of different levels of canopy drag-force prescription on flow modelling

6.2.1 Initialization

As mentioned above, in order to explore the effect of different levels of canopy drag-force prescription on air flow modelling over forested terrain we consider a limited domain with flat topography. Detailed views of space distribution of tree heights and PAI are given in Fig. 11a and in Fig. 11b, respectively. As mentioned above, for airflow modelling with full implementation of canopy drag the PAD profiles given by Eq. (2) with α = 3 and β = 3 were used. A roughness of forest floor was set to 0.1 m. For airflow modelling based on a single parameter the effective roughness given in Fig. 10a was used. Simulations using Ellipsys3D solver were performed using the horizontal resolution of 16 m, while SCADIS simulations were performed using the horizontal resolution of 48 m.

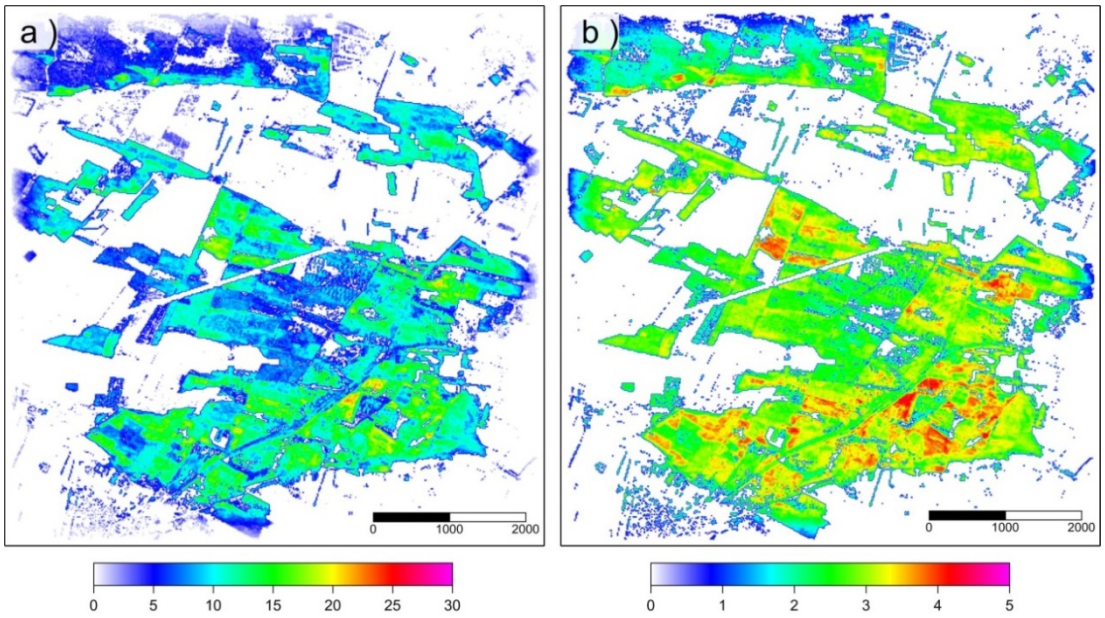

Figure 11. The vegetation height, *h* (m) (a) and plant area index, PAI (m^2 m^{-2}) (b) in a limited domain used for airflow modelling.

6.2.2 Wind speed simulations

The results of the numerical experiments presented in Figs. 12, 13 and 14 show that both models with different parameterization of the vegetation effect produce similar wind speeds over the investigated domain. Effects of vegetation on the flow are clearly seen. When using the canopy drag parameterization, both models, especially EllipSys3D (Figs. 12 and 13), provide more details on wind speed at the height of 25 m, but with increasing the height wind speed becomes smoothed. When using the effective roughness, both models provide smoothed wind speed at all levels considered in the analysis. Some differences in results between the two models do however exist (for further elaboration of this issue see Sogachev et al. 2015). Here we focus on how each specific model copes with air flow modelling using different vegetation representation.

The scatter plot in Fig. 15 shows that the CFD solution based on $z_{0,eff}$ is not applicable at low elevations for both models. Wider scatter in resulted data for EllipSys3D (both with k - ω and k - ε closures) can be due to higher canopy resolution used in this model and as such due to introduction of more details in the calculations. Also it can be explained by different numerical methods applied in SCADIS and EllipSys3D. With increase in height, the difference in wind speed derived using different parametrizations becomes smaller, and scatter points increasingly converge towards the 1 : 1 line (see Fig. 15), except for EllipSys3D based on k - ε closure. Wind speed derived using the z_{0eff}-approach is always higher than that derived using the full canopy drag implementation. Besides general differences in the results due to different closures (Sogachev et al. 2015), this result can indicate a possible problem of correct estimation of $z_{0,eff}$ for this type of closures. Note that results demonstrated by SCADIS (smaller scatter) are in better agreement than results of EllipSys3D solver. The reason of that can be that derivation of $z_{0,eff}$ have been done based on SCADIS solution itself. Some other reasons will be discussed later (see Section 7).

Figure 16 show the wind speed estimated by SCADIS along the west-east transect over the area indicated in Fig.12 (dashed lines). One can see that the large difference in estimated wind speed fields is observed in lowest layer of atmosphere and of course inside the layer occupied by vegetation. With increase the height (z), the difference becomes smaller and at some height the solutions of two models match each other.

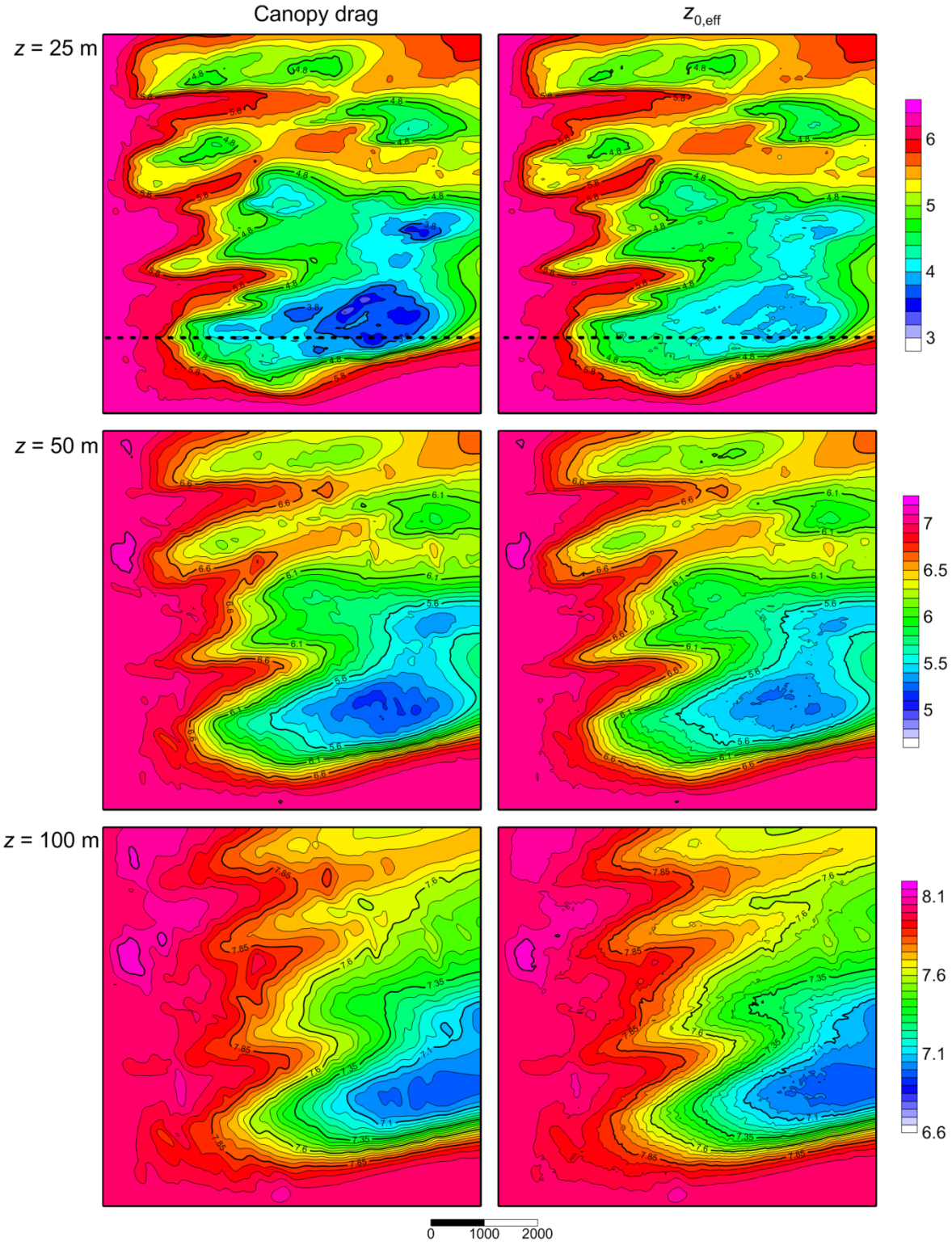

Figure 12 *. Wind velocity (m s^{-1}) at different heights modelled by SCADIS using the canopy drag (on the left side) and the effective roughness (on the right side). Dashed lines in the upper panel indicate transects, the results of modelling along which presented in Fig.16.*

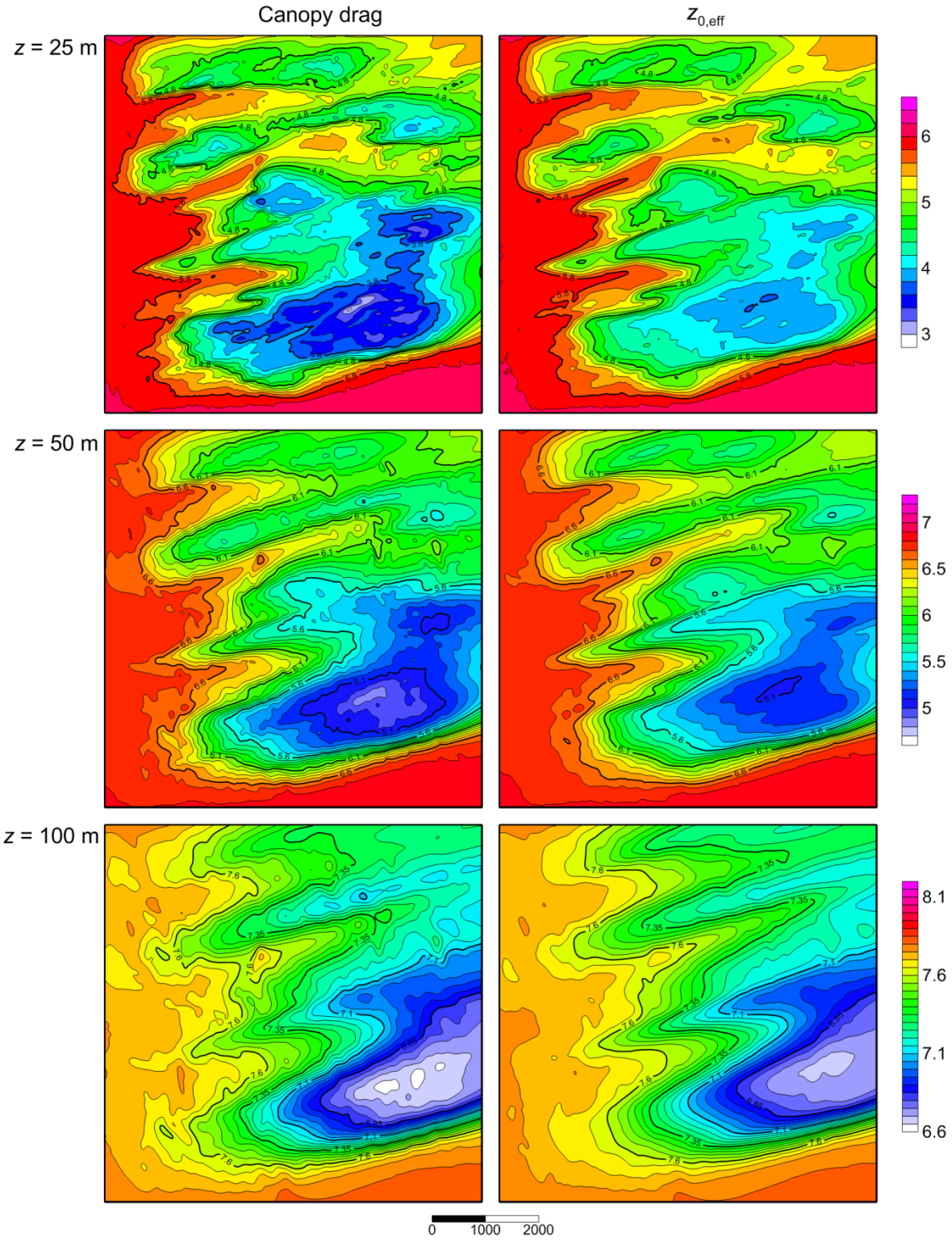

***Figure 13**. Wind velocity (m s^{-1}) at different heights modelled by EllipSys3D (k - ω closure) using the canopy drag (on the left side) and the effective roughness (on the right side).*

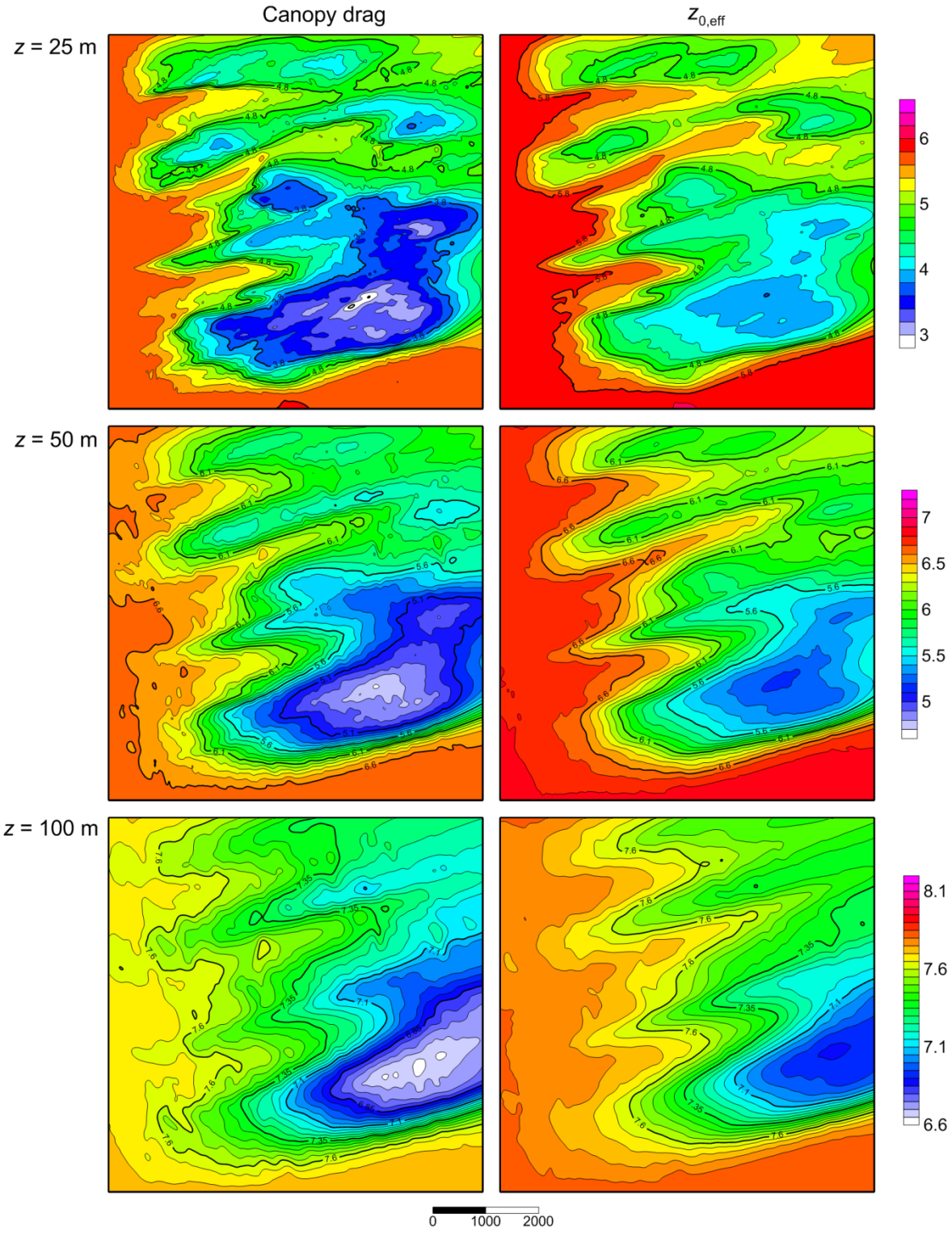

***Figure 14**. Wind velocity (m s^{-1}) at different heights modelled by EllipSys3D (k - ε closure) using the canopy drag (on the left side) and the effective roughness (on the right side).*

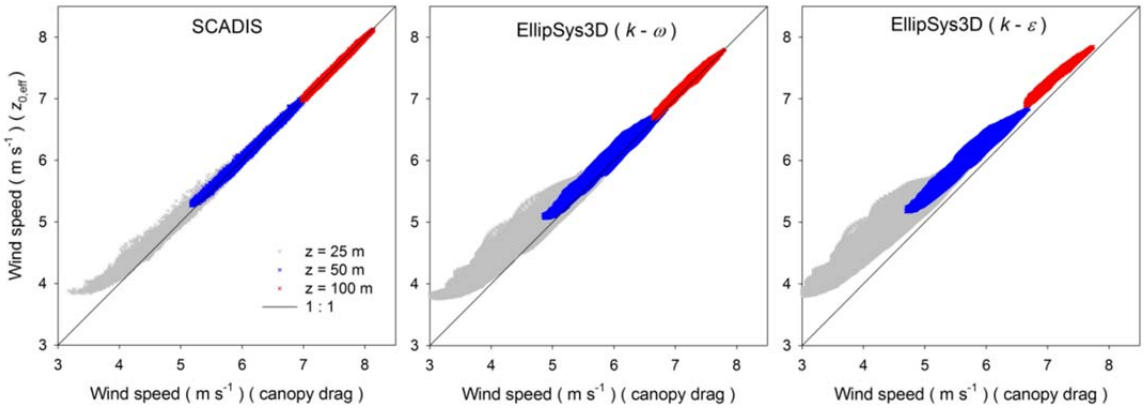

Figure 15. *Wind speed at 25 m AGL (grey), at 50 m AGL (blue) and at 100 m AGL (red) derived by different models with canopy drag against that derived by models with the effective roughness over the modelling domain. The 1 : 1 line is also shown.*

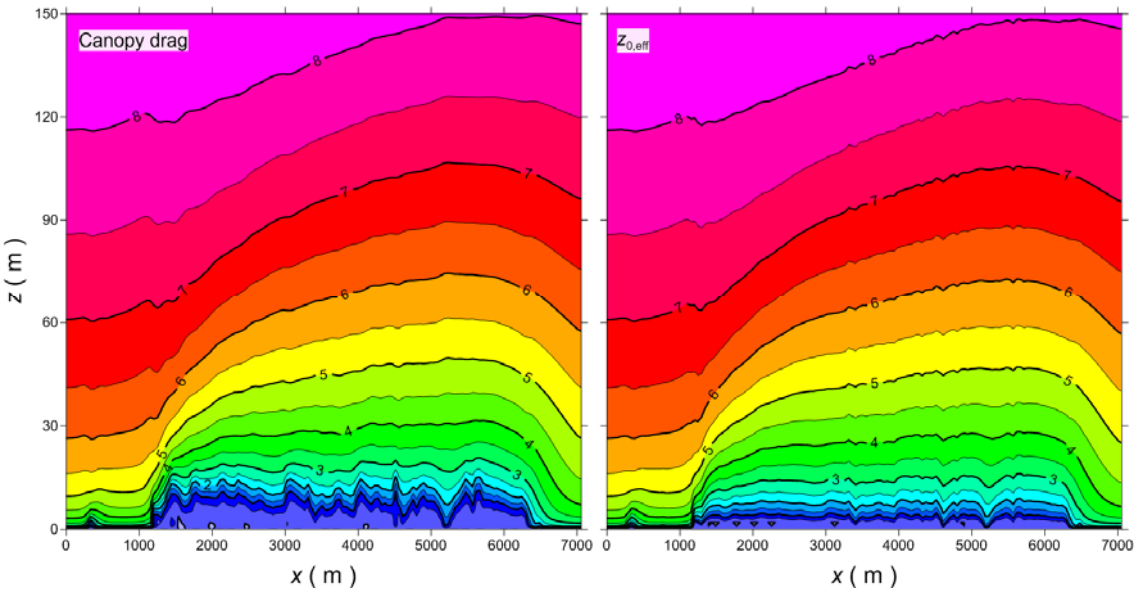

Figure 16*. Wind velocity (m s^{-1}) along the west-east transect (see location in Fig. 12) modelled by SCADIS using the canopy drag (left panel) and the effective roughness (right panel).*

6.2.3 TKE simulations

Results for turbulent kinetic energy (TKE) resolved by using two modelling approaches for vegetation show also a reasonable agreement between the two models (Figs. 17, 18 and 19). Both models seem to describe the effect of vegetation on turbulence in a similar way, even though some differences in absolute values of calculated TKE can be seen (especially for EllipSys3D based on k - ε closure). One can observe indeed, that the forest increases turbulence intensity. The areas of high values of TKE are located just above the forest and spread downwind with the increasing height. The areas with denser and higher forest (see also Figs. 10 and 11) indicate the larger effect on the TKE production. The scatter plot of TKE data (Fig. 20) also shows that with height, the difference in turbulence levels calculated utilizing two different approaches in the two models becomes a minor one. As in a case of the wind speed, again the SCADIS results demonstrate a smaller scatter. Ellipsys3D (k - ε) results demonstrate that besides larger scatter, the TKE estimated by this model using effective roughness approach is smaller than TKE estimated using canopy drag approach. Reasons for that and possible ways of improvement will also be discussed below.

As a whole, the results of numerical experiments show that CFD approach based on $z_{0,eff}$ vegetation representation can do good work in estimation of air flow speed and turbulence level over forested area at heights potentially interesting for wind industry applications (100 m and higher).

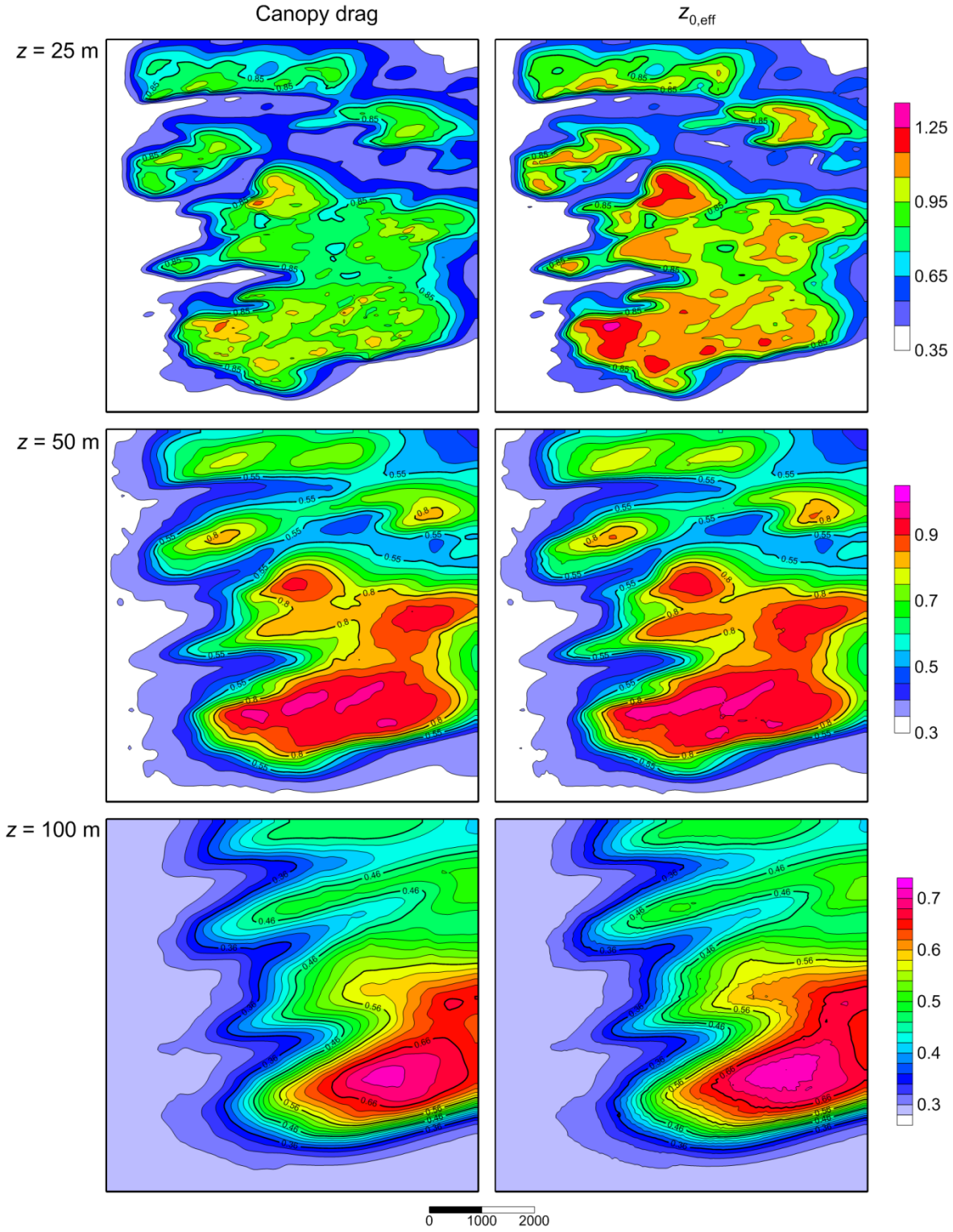

Figure 17. *Turbulent kinetic energy (m^2 s^{-2}) at different heights above the ground modelled by SCADIS using the canopy drag (on the left side) and the effective roughness (on the right side).*

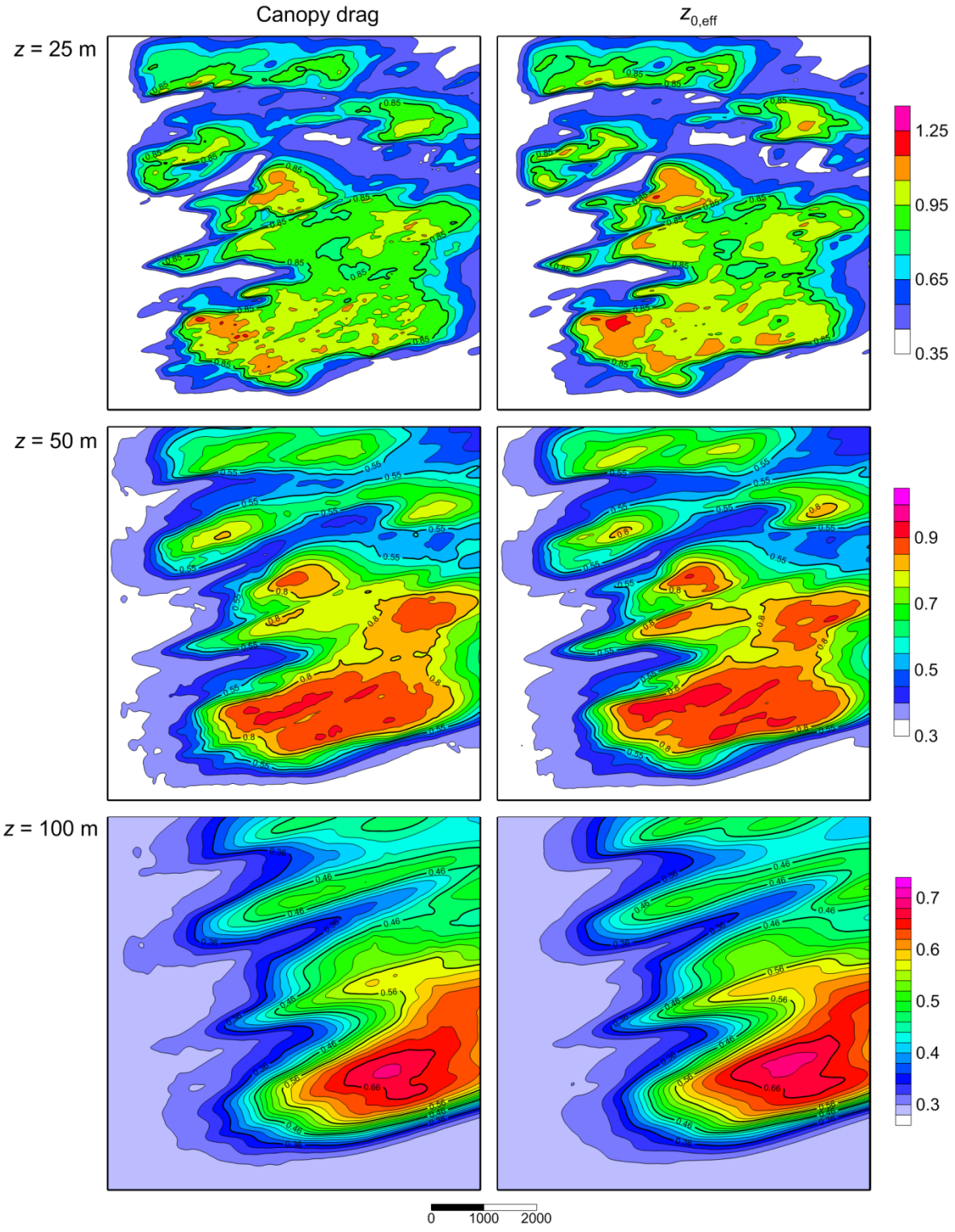

Figure 18. *Turbulent kinetic energy ($m^2\ s^{-2}$) at different heights above the ground modelled by EllipSys3D (k - ω closure) using the canopy drag (on the left side) and the effective roughness (on the right side).*

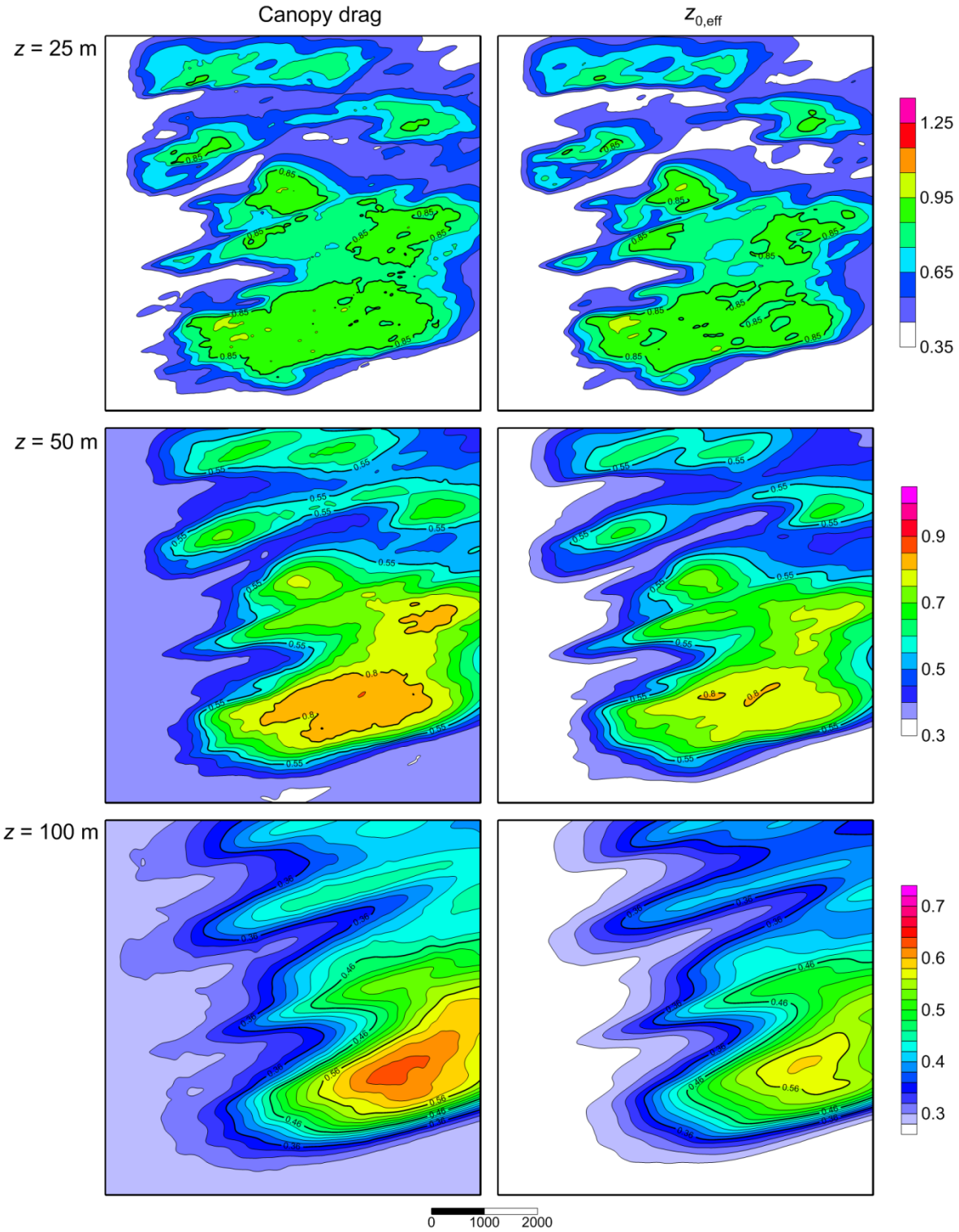

Figure 19. *Turbulent kinetic energy (m^2 s^{-2}) at different heights above the ground modelled by EllipSys3D (k - ε closure) using the canopy drag (on the left side) and the effective roughness (on the right side).*

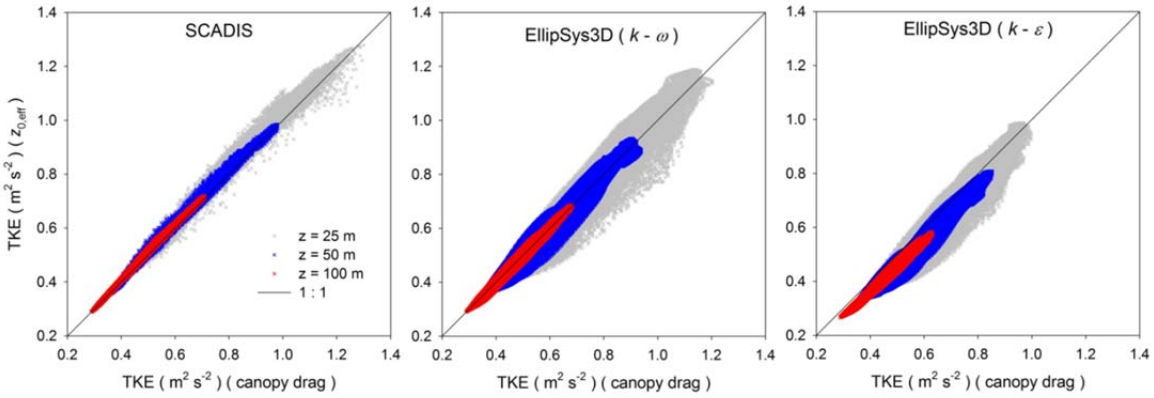

***Figure 20**. TKE at 25 m AGL (grey), at 50 m AGL (blue) and at 100 m AGL (red) derived by different models with canopy drag against that derived by models with the effective roughness over the modelling domain. The 1 : 1 line is also shown.*

7. Discussion

There are several issues that should be addressed and further tested, in order to assess how well the presented simplified canopy description describes flow over forested areas. In the following we outline some of the primary issues.

Forest data. Though we test the approach using simplified representation of real forested terrain, the approach is applicable for initial information about vegetation of any complexity. For example, the growing interest in LiDAR scans seems to promise finer resolution and improved post-processing algorithms, which will eventually provide a better description of the forest structure, and consequently better output from our approach. Having high-resolution information from LiDAR scans allows for classification of data with any height graduation. Decreasing the number of classes increases the number of PAD profiles in each class, effectively smoothing the resultant profiles. It should be kept in mind that sparse but high vegetation types, which are typical for clear-cuts, roads or power lines can produce unrealistic high values of the effective roughness. The solution can be to separate, behind height classes, vegetation into two PAI groups to correctly keep areas with low PAI. We also advise to test different thresholds of PAI and tree height for which a given vegetation class can be replaced by an open-place class.

Empirical methodology. Two methods have been widely used for the representation of PAD with minimum information about the tree structure. For dense and high forest the methods provide similar shapes of vertical PAD (see Fig. 1) that will probably cause only minor differences in resulting wind profiles. One advantage of the method based on the beta probability (Meyers and Paw U, 1986) is, that for any set of non-negative α and β parameters, the real plant area density depends only on the information about PAI. The method proposed by Lalic and Michailovic (2004) needs information about PAD_m to get profiles and must be corrected to provide the PAI needed.

Reduced-dimensionality and consistency with geostrophic drag law. Because the SCADIS model has been validated extensively against different types of vegetation (e.g. Sogachev and Panferov, 2006), we do not anticipate issues with its representation of basic flow statistics inside the canopy. A minor unresolved issue is the choice of geostrophic drag-law coefficients A and B used in equations (6) and (7). Both values are within the ranges given in the literature, with B being slightly higher than typically-used values. The advanced turbulence model implementation in SCADIS can be adjusted to satisfy classical B values, but without conducting comprehensive tests, it is difficult to say whether the model will still reproduce canopy flow correctly. Here for simplicity we use fitted values that provide a match of the SCADIS simulations with the vertically distributed canopy drag, and only with $z_{0,eff}$ defined from equation 7 (see Figs. 6 and 7). Also, it is important to note that the resultant $z_{0,eff}$ is a function of the wind speed; this is a feature resulting from inclusion of the Coriolis force (among other things). Thus application of derived $z_{0,eff}$ to different wind conditions at given site will also be tested. Further, the aggregate drag and apparent geostrophic-scale roughness should be consistent, regardless of the number of dimensions of the simulation (at least for homogeneous forest statistics).

CFD flow modelling. There is still a need for more numerical experiments to test the sensitivity of flow modelling to different distributions of $z_{0,eff}$,also including topographical effects. One of possible solution to get quick estimates of flow over forested terrain is application of a mass-consistent model (e.g. Sherman 1978). The first guess about wind distribution can be done based one estimation of ABL profiles from reduced-dimension CFD, which can be also combined in lower part of ABL with log-law profile based on estimates of d and z_0. There are problems with the k - ε closure, relative to the k - ω; to estimate the better results we need to use EllipSys3D with extra diffusion term (following Sogachev et al., 2012; 2015). There is also another possibility, to estimate effective roughness using a one-dimensional k - ε model. There are questions about how different closures behave regarding the effective roughness. Sogachev et al (2012) showed that k - ω and k - ε in classical forms provide different results in canopy flow modelling. Thus it should be also difference if we replace the canopy by effective roughness, maybe the difference will be more pronounced and this happened in present study.

Filtering and smoothing data. To get a distribution of classes with resolution coarser than that given by initial PAD data and especially in the case of fine LiDAR scan data, two options do exist. Option 1 would be to use aggregated PAD values inside the coarse cell. Option 2 would be to use classes derived on a small-resolution grid. A simple aggregation of classes inside larger cell is incorrect, but we can aggregate dynamical properties of classes such as effective roughness, displacement height or aerodynamic roughness. Aggregated values of effective roughness can be used on finer grids directly, but do not allow us to identify vegetation classes. Using the information about the aggregated displacement height and subgrid roughness variation (within cells) helps, because these two parameters, in contrast to $z_{0,eff}$, are unique for each class.

8. Conclusions

We present a CFD method to facilitate use of forest data of any level of detail in flow models with different types or levels of canopy drag-force prescription. Preliminary numerical tests showed that CFD models with different levels of canopy drag-force prescription provide similar results on both wind field and TKE level beginning from the some height over ground surface (z/h > 3-5). The method also allows for consistent comparison with known theory, measurements, and commonly-used parameters in forest-flow modelling. The spatial information about effective roughness can be used as input, not only for CFD models, but also for mesoscale or linearized models. In order to easily use the derived information in such models, we suggest applying a bilateral filter (e.g. Tomasi and Manduchi, 1998) for smoothing the parameters over the area considered; smoothing of aerodynamic parameters is more physically-based than smoothing of discrete land-use classes.

References

Arnqvist J, Segalini A, Dellwik E, Bergström H. 2015 Wind statistics from a forested landscape. Boundary-Layer Meteorology. 156(1):53-71

Blackadar A. K., Tennekes H., 1968 Asymptotic similarity in neutral barotropic planetary boundary layers J. Atmos. Sci. 25 1015–20

Boudreault L-É, Bechmann A, Tarvainen L, Klemedtsson L, Shendryk I., Dellwik E., 2015 A LiDAR method of canopy structure retrieval for wind modeling of heterogeneous forests Agric. For. Meteorol. 201 86–97

Breuer L., Eckhardt K., Frede H-G., 2003 Plant parameter values for models in temperate climates. Ecol Model 169 237–93

Cermák, J., Riguzzi, F., Ceulemanns R., 1998 Scaling up from individual tree to the stand level in Scots pine. I. Needle distribution, overall crown and root geometry. Annales des Sciences Forestières 55, 63-88

Clarke R H., Hess G D., 1974 Geostrophic departure and the functions A and B of Rossby-number similarity theory, Boundary-Layer Meteorol. 7 261-87

Lalic B., Mihailovic D. T., 2004 An empirical relation describing leaf-area density inside the forest for environmental modeling J. Appl. Meteorol. 43 641–5

Lefsky MA, Cohen W B, Acker S, Parker GG, Spies T A., Harding D., 1999 Lidar remote sensing of the canopy structure and biophysical properties of Douglas-fir western hemlock forests. Remote Sens. Environ. 70 339–61

Mann, J., Courtney, M., Hummelshøj, P., Hjuler Jensen, P., 2010 Undersøgelse af vindforhold ved det kommende testcenter ved Østerild. Roskilde: Danmarks Tekniske Universitet, Risø Nationallaboratoriet for Bæredygtig Energi. (Denmark. Forskningscenter Risoe. Risoe-R; Nr. 1743(EN)).

Markkanen T, Rannik Ü, Marcolla B, Cescatti A., Vesala T., 2003 Footprints and fetches for fluxes over forest canopies with varying structure and density Boundary-Layer Meteorol. 106 437–59

Melgarejo J W., Deardorff J. W., 1974 Stability functions for the boundary layer resistance laws based upon observed boundary layer height. J. Atmos. Sci. 31 1324-33

Meyers T., Tha Paw U. K., 1986 Testing of a higher-order closure model for modeling airflow within and above plant canopies Boundary-Layer Meteorol. 37 297–311

Michelsen J A. 1992 Basis3d – a platform for development of multiblock pde solvers. Technical report AFM 92-05. Technical University of Denmark.

Morsdorf F, Kotz B, Meier E, Itten K I., Allgower B., 2006 Estimation of LAI and fractional cover from small footprint airborne laser scanning data based on gap fraction Remote Sens. Environ. 104 50–61

Nebenführ B., Davidson L., 2015 Large-eddy simulation study of thermally stratified canopy flow Boundary-Layer Meteorol. 156 253–76

Picard N., Saint-André L., Henry M. 2012. Manual for building tree volume and biomass allometric equations: from field measurement to prediction. 215pp. Food and Agricultural Organization of the United Nations, Rome, and Centre de Coopération Internationale en Recherche Agronomique pour le Développement, Montpellier. [12].

Pope S B., 2000 Turbulent flows. 771 pp. Cambridge University Press, United Kingdom.

Pretzsch, H., P. Biber, J. Dursky. 2002. The single tree-based stand simulator SILVA: construction, application and evaluation. Forest Ecology and Management 162, 3-21.

Raupach M R., 1992 Drag and drag partition on rough surfaces Boundary-Layer Meteorol. 60 375–95
Raupach M R., 1994 Simplified expressions for vegetation roughness length and zero-plane displacement as functions of canopy height and area index Boundary-Layer Meteorol. 71 211–16
Richardson J J, Moskal L M., Kim SH., 2009 Modeling approaches to estimate effective leaf area index from aerial discrete-return LIDAR Agric. Forest Meterol 149 1152–60.
Ross, J. 1981 The Radiation Regime and Architecture of Plant Stands. 391 pp. Springer, Dordrecht, Netherlands.
Sherman, C.A. 1978 A mass consistent model for wind field over complex terrain. Journal of Applied Meteorology, 17, 312–319.
Siipilehto, J., 2000 A comparison of two parameter prediction methods for stand structure in Finland. Silva Fennica 34 (4), 331-349.
Sogachev A., Menzhulin G.V., Heimann M., Lloyd J., 2002 A simple three-dimensional canopy - planetary boundary layer simulation model for scalar concentrations and fluxes Tellus B 54 784–819
Sogachev A., Panferov O., 2006 Modification of two-equation models to account for plant drag Boundary-Layer Meteorol. 121 229–66
Sogachev A., 2009 A note on two-equation closure modelling of canopy flow Boundary-Layer Meteorol. 130 423–35
Sogachev A., Kelly M.C., Leclerc M.Y., 2012 Consistent two-equation closure modelling for atmospheric research: buoyancy and vegetation implementations". Boundary-Layer Meteorol 145(2):307-327.
Sogachev, A., Cavar, D., Bechmann, A., Jørgensen, H.E., 2015 Assessment of consistent two-equation closure for forest flows. Abstract from EWEA Annual Conference and Exhibition 2015, Paris, France.
Sogachev A., Kelly M., 2016 On displacement height, from classical to practical formulation: stress, turbulent transport and vorticity considerations Boundary-Layer Meteorol. 158 361–81
Solberg, S, Næsset E, Hanssen K H., Christiansen E., 2006 Mapping defoliation during a severe insect attack on Scots pine using airborne laser scanning Remote Sens. Environ. 102 364–76
Sørensen NN. 2003 Tech. Rep. Risø-R-827(EN), 154 pp, Risø National Laboratory.
Tomasi C., Manduchi R., 1998 Bilateral filtering for gray and color images Int. Conf. Comput. Vis. 839–46
Troen I., Petersen E L., 1989 The European Wind Atlas. Published for the Commission of the European Communities, Directorate-General for Science, Research, and Development, Brussels, Belgium by Risø National Laboratory 656 pp
Van Den Hurk B J J M, McNaughton K G., 1995 Implementation of near-field dispersion in a simple two-layer surface resistance model J. Hydrol. 166 293–311
Widlowski JL., Verstraete M.,Pinty B., Gobron N., 2003 Allometric relationships of selected European tree species 63pp., EC Joint research centre, TP 440, I-21020 Ispra (VA), Italy.

Appendix A Allometric relationships for Scots Pine

The plantation surrounding Østerild area today consists mainly of Scotch pine, mountain pine, silver fir, sitka spruce and common spruce with smaller areas of beech, oak and birch. Also many varieties of dwarf shrubs can be found such as bog bilberry, crowberry, heather, bell heather and bog myrtle (http://green.thisted.dk). For simplicity we accept assumption that all trees at the site are Scots Pines and to produce the information needed for modelling such as PAD we apply some allometric equations describing tree architectural properties for Scots pine (*Pinus sylvestrics*) (see Widlowski et al., 2003). The DBH (Diameter-at-Breast-Height) parameter is commonly expressed in units of centimetres [cm], whereas most of the allometrically derived quantities retain their SI units, i.e., they are expressed in units of metres [m]. Given review of existing allometric relationships for Scots pine, Widlowski et al., 2003 recommended the next expressions for the total tree height, *h* (Siipilehto, 2000)

$$h = 1.3 + \left(\frac{DBH}{0.894 + 0.185 DBH} \right)^2 [\mathrm{m}], \tag{A.1}$$

and PAI (Cermák et al., 1998)

$$\mathrm{PAI} = \exp(0.375) DBH^{0.375} [\ ]. \tag{A.2}$$

Having as input information about *h* we can estimate DBH and after that PAI as a function of tree height. The problem of expression (A.1) that *h* arrives the upper tree height limit around 26 m that will give a very large PAI values, for trees higher than 20 m. We suggest a simplified expression for PAI as function of *h*

$$\mathrm{PAI} = 5\sqrt{h/30\mathrm{m}}\ . \tag{A.3}$$

Eq. (A.3) is in a good agreement with Eqs. (A.1) and (A.2) for tree height till 20 m and provides also reasonable solution for higher heights (see Fig. 21).

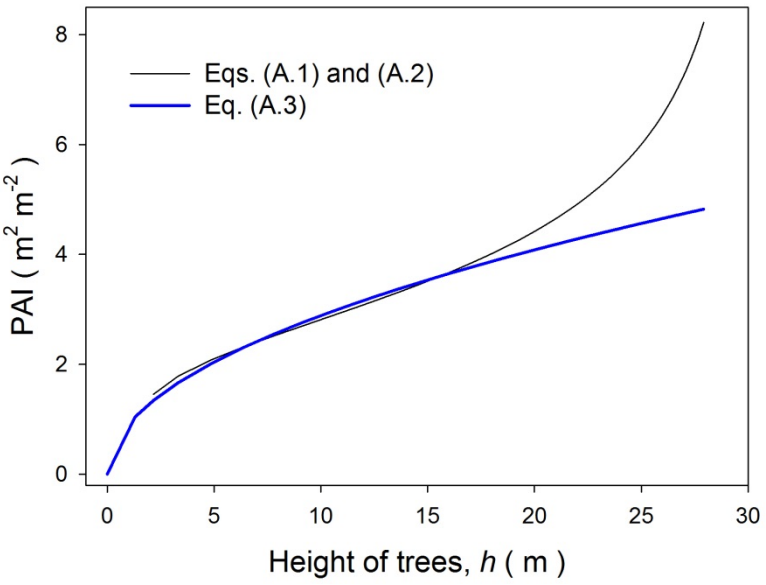

Figure 21*. The Plant Area Index (PAI) for Scots pine when derived from the allometric relationships (A.1) and (A.2) and the simplified expression (A.3) as function of the tree height.*

Eq. (A.3) provides also a good agreement with experimental data about PAI for a forested region near Ryningsnäs in the south-east of Sweden located approximately at the same latitude as Østerild. According to Arnqvist et al. (2015) the forest is consisted predominantly of Scots pine (Pinus silvestris) and the average forest height is approximately 20 m. Nebenführ and Davidson (2015) successfully modelled wind flow over this area with PAI = 4.3.

The heights (z_m) where maximum plant area density PAD_m occurs is a cruisial parameter in derivation of PAD profile. Pretzsch et al. (2002) indicates that the height to the maximum crown width for Scots pine can be approximated by $z_m = 0.5(h+h_t)$, where h_t is the height to the tree crown, given as

$$h_t^* = h\left(1-\exp^{\left(0.376-0.9963\frac{h}{DBH}-0.0218\,DBH\right)}\right)\left[\mathrm{m}\right]. \qquad \text{(A.4)}$$

However, Widlowski et al. (2003) pointed out that this allometric formulation makes that h_t is almost equal to the tree height h at low DBH values thus almost completely eliminating the crown length. To account for the fact that the crown of young trees often extends almost to the ground, Cermák et al. (1998) provided the following relationship

$$h_t^{**} = 16.9\left(1-\exp^{\left(\frac{DBH}{3.45}\right)}\right)^{9.513}\left[\mathrm{m}\right]. \qquad \text{(A.5)}$$

As it seen this realtionship has a upper limit for the crown height. As solution we used the geometrical mean of this two expression. Thus the normalized height with maximul PAD value was derived as

$$\frac{z_m}{h} = \frac{1}{2} + \frac{\sqrt{h_t^* \times h_t^{**}}}{2}, \tag{A.6}$$

where h is given by Eq. (A.1). The behaviour of this function as function of h is shown in Fig. 22. Assuming that after achieving its maximum the value z_m/h does not change we parameterize the behaviour of z_m/h by the sigmoidal five parameters equation

$$\frac{z_m}{h} = 0.4922 + \frac{0.398}{\left(1+\exp\left(-\left(h-8.5174\right)/2.5499\right)\right)^{1.2872}}, \tag{A.7}$$

which is also presented in Fig. 22.

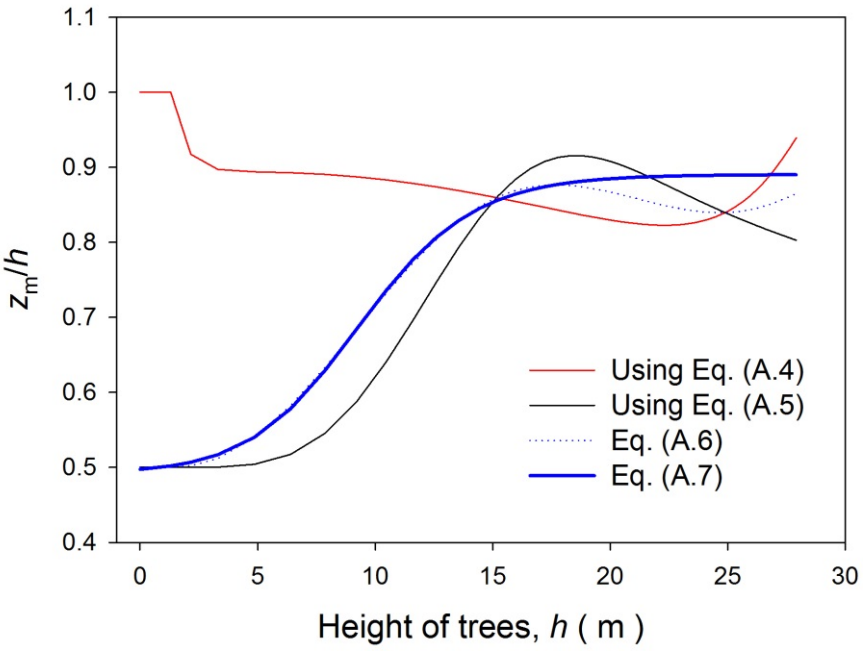

***Figure 22**. The normalized heights of maximal values of PAD derived by using different allometric relationships and using the empirical fit.*

The expression (A.7) can be directly applicable in Eq. (4) for estimation of α under some assumption of values β (usually accepted as 3). Together with Eq. (A.3) that further provides PAD profile simply as function of h from Eq. (2). Using of Eq. (6) is still difficult so far as no information about values of PAD_m is known.

DTU Wind Energy is a department of the Technical University of Denmark with a unique integration of research, education, innovation and public/private sector consulting in the field of wind energy. Our activities develop new opportunities and technology for the global and Danish exploitation of wind energy. Research focuses on key technical-scientific fields, which are central for the development, innovation and use of wind energy and provides the basis for advanced education at the education.

We have more than 250 staff members of which approximately 40 are PhD students. Research is conducted within nine research sections and five programmes.

Technical University of Denmark
Department of Wind Energy
Frederiksborgvej 399
Building 118
4000 Roskilde
Denmark
Telephone 46 77 50 85

info@vindenergi.dtu.dk
www.vindenergi.dtu.dk